Enhancing Distribution System Resilience With Mobile Energy Storage and Microgrids

Jip Kim, *Student Member, IEEE*, and Yury Dvorkin, *Member, IEEE*

***Abstract*—Electrochemical energy storage (ES) units (*e.g.*, batteries) have been field-validated as an efficient back-up resource that enhances resilience of distribution systems. However, using these units for resilience is insufficient to justify their installation economically and, therefore, these units are often installed in locations where they yield the greatest economic value during normal operations. Motivated by the recent progress in mobile ES technologies, *i.e.*, ES units can be moved using public transportation routes, this paper proposes using this spatial flexibility to bridge the gap between the economically optimal locations during normal operations and the locations where extra back-up capacity is necessary during disasters. We propose a two-stage optimization model that optimizes investments in mobile ES units in the first stage and can re-route the installed mobile ES units in the second stage to form dynamic microgrids (MGs) and to avoid the expected load shedding caused by disasters. Since the proposed model cannot be solved efficiently with off-the-shelf solvers, even for relatively small instances, we apply the progressive hedging algorithm. The proposed model and algorithm are tested on a 15-bus radial distribution test system.**

***Index Terms*—Mobile energy storage, grid resilience, microgrid, distribution system, progressive hedging.**

NOMENCLATURE

Sets and Indices

$b \in \mathcal{B}$	Set of buses
$k \in \mathcal{K}$	Set of energy storage units
$l \in \mathcal{L}$	Set of distribution lines
$s \in \mathcal{S}$	Set of scenarios
$t \in \mathcal{T}$	Set of time intervals.

Parameters

$\aleph^{\mathrm{ch/dis}}$	Charging/Discharging efficiency
α_{lts}	Contingency parameter of line l
γ	Daily capital recovery factor
ω_s	Probability of scenario s
h	Degradation slope of energy storage units
$r(l)$	Receiving-end bus of line l
$s(l)$	Sending-end bus of line l
$\overline{E}_k$	Energy rating of energy storage units [MWh]
$\overline{P}_k$	Power rating of energy storage units [MW]
B_b	Susceptance of bus b [Ω^{-1}]
C^{E}	Energy rating price of energy storage units[\$/MWh]
C^{g}_b	Incremental cost of distributed generator [\$]
C^{P}	Power rating price of energy storage units [\$/MW]
C^{VoLL}_b	Value of lost load [\$/MWh]
G_b	Conductance of bus b [Ω]
K	Power factor calculation coefficient
N^{B}	The number of buses
N^{DG}	The number of distributed generators
N^{ES}	The number of mobile energy storage units
N^{L}	The number of distribution lines
N^{O}	The number of lines in outage
N^{S}	The number of scenarios
N^{T}	The number of time intervals
P^{d}_{bts}	Real power demand [MW]
Q^{d}_{bts}	Reactive power demand [MVar]
R_l	Resistance of distribution line l [Ω]
S_l	Apparent flow limit of distribution line l [MVA]
X_l	Reactance of distribution line l [Ω].

Binary Variables

$\sigma^{\mathrm{d}}_{bts}$	Load switch state variable: 1 if load at bus b is connected to bus, 0 otherwise
$\sigma^{\mathrm{l}}_{lts}$	Line switch state variable: 1 if line l is closed, 0 otherwise
u_{kbts}	Transit route variable of ES unit in mobile mode: 1 if ES unit k is located at bus b, 0 otherwise.
x_k	Investment decision variable of energy storage unit: 1 if energy storage unit k is installed, 0 otherwise
z_{kb}	Stationary location variable of ES unit: 1 if ES unit k is located at bus b, 0 otherwise.

Variables

a_{lts}	Squared current flow of distribution line l [p.u.]
e_{kts}	Energy state-of-charge [MWh]
$f^{\mathrm{p/q}}_{lts}$	Real/Reactive power flow of line l [MW/MVar]
$p^{\mathrm{ch/dis}}_{kbts}$	Charging/Discharging real power decision [MW]
p^{g}_{bts}	Real power output of distributed generator [MW]
$q^{\mathrm{ch/dis}}_{kbts}$	Charging/Discharging reactive power decision [MVar]
q^{g}_{bts}	Reactive power output of distributed generator [MVar]
v_{bts}	Squared nodal voltage magnitude of bus b [p.u.]
IC	Investment cost [\$]

Manuscript received April 7, 2018; revised August 16, 2018; accepted September 25, 2018. Date of publication September 28, 2018; date of current version August 21, 2019. This work was supported by U.S. NSF under Grant ECCS-1760540. Paper no. TSG-00528-2018. *(Corresponding author: Jip Kim.)*

The authors are with the Department of Electrical and Computer Engineering, Tandon School of Engineering, New York University, New York, NY 11201 USA (e-mail: jipkim@nyu.edu).

Color versions of one or more of the figures in this paper are available online at http://ieeexplore.ieee.org.

Digital Object Identifier 10.1109/TSG.2018.2872521

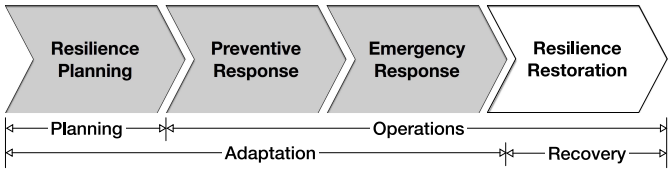

Fig. 1. The resilience enhancement steps [4] and the scope of this paper (shaded).

EC_s Emergency cost of scenario s [$]
OC_s Operation cost of scenario s [$].

I. Introduction

THE U.S. power grid is vulnerable to natural disasters (*e.g.*, flooding, extreme winds, earthquakes) as they increase the likelihood of critical equipment failures [1]. Distribution systems are particularly affected by natural disasters due to the compounding effect of line outages, radial topology, and limited back-up resources. Furthermore, a large-scale disaster can affect a power grid in multiple locations causing the domino effect, which may in turn spread power outages across large geographical areas, even if some areas would not otherwise be affected by the disaster [2]. Therefore, it is important to contain the failures within distribution systems and prevent their further propagation to the transmission system.

To continue operating and delivering power even in case of such low probability, high-consequence events as hurricanes and earthquakes [3], power grid resilience can be enhanced by means of planning, response, and restoration. The response step may be divided into preventive and emergency responses based on whether it is prior to or after the event strikes. Fig. 1 illustrates this classification and functional objectives of each step. In the planning stage, a distribution system operator (DSO) builds a long-term investment plan of generation resources and facility hardening. Utilizing such grid assets, the DSO is better suited to accommodate abnormal conditions caused by natural disasters (*i.e.*, adaptation) or to restore the normal system condition (*i.e.*, recovery). The objective of this paper is to illustrate that mobile energy storage (ES) units are also economically and physically suitable for the adaptation stage and thus enhance distribution resilience. For this purpose, we propose an investment model that includes a joint allocation and operation strategy for the mobile ES units with microgrid (MG) formation.

A mobile ES unit, often referred to as "storage-on–wheels," is an emerging technology that takes the form of a trailer-mounted electrochemical battery. Consolidated Edison of New York is currently considering installing such mobile ES units to reduce the impact of PV generation on their distribution system in New York City and defer costly distribution upgrades [5]. As reported in [5], each mobile ES unit will feature a Lithium-ion battery that can store up to 800 kWh of energy with the maximum charging/discharging duration of 10 hours. Compared to other resilience response resources, the mobile ES units have multiple advantages. First, they are more environmentally friendly than portable emergency generators and can be used without unnecessary noise and air pollution. Furthermore, strict pollution standards in certain jurisdictions, especially in metropolitan areas, prohibit the use of portable emergency generators during normal operations, which reduce their value to the distribution system. Second, unlike preventive load shedding or adaptive microgrids, the mobile ES units can be directly operated by the power grid operator and do not require advanced communication infrastructure or engagement with electricity consumers. Since the capital cost of ES units is relatively high, it is important to ensure their economic viability. Exploiting ES mobility for resilience applications can enhance its value to the grid and create new revenue streams to accelerate its cost recovery.

TABLE I
Survey of Previous Studies

	Formulation	Power Flow	DG	ES	MG	Resilience Stage	Mobility of Resources
[4]	MILP	DC-OPF	✓	-	-	Response	-
[8]	MILP	DC-OPF	✓	-	-	Response	-
[9]	MILP	DC-OPF	✓	✓	✓	Planning	-
[10]	-	FB Sweep	✓	-	✓	Planning	-
[11]	MINLP	AC-OPF	✓	✓	✓	Response	-
[12]	MIQP	LinDistFlow	✓	-	✓	Response	✓
[13]	MILP	LinDistFlow	✓	-	✓	Planning	✓

* DG: Distributed Generator, ES: Energy Storage, MG: Microgrid

Provided there is a timely disaster forecast, the SO can prevent critical failures, or at least mitigate their impacts, by strategically placing flexible back-up resources (*i.e.*, mobile storage) [6]. Since the disaster forecasts are normally available on a short notice (for instance, NOAA forecasts are available 48-168 hours ahead [7]), only a few alternative technologies are physically suitable to be deployed, relocated or activated within this timeframe: portable emergency generators, topology switching, preventive load shedding, or adaptive microgrid. Table I presents the previous literature on such technologies and their comparison. Huang *et al.* [4] propose an integrated method to utilize topology switching and preventive load shedding for resilience response. Wang *et al.* [8] devise a proactive operation strategy with topology switching and generation re-dispatch through the Markov process. Zhang *et al.* [9] formulate a planning problem that optimizes sizing and siting of the photovoltaic generation and storage. Nassar and Salama [10] describe an adaptive self-adequate microgrid planning with flexible boundaries. Wang and Wang [11] develop a self-healing strategy by partitioning a given distribution system into self-adequate microgrids. The common thread of [4] and [8]–[10] is that they consider stationary resilience resources. Lei *et al.* [12] consider mobile emergency generators and microgrid formation in a mixed-integer quadratic program (MIQP). Accordingly, the model in [12] formulates two separate optimization problems that sequentially pre-position and route mobile emergency generators in real-time. Due to this separation, the pre-positioning decisions are informed of the routing decisions and thus might be sub-optimal. Sedzro *et al.* [13] describe a similar planning framework considering controllability of demand

response and mobility of distributed generators (DGs), leading to a mixed-integer linear program (MILP). However, the models in [12] and [13] disregard multi-temporal constraints, while optimizing their planning decisions, and therefore are not suitable for modeling ES units.

A typical state-of-the-art planning tool for stationary ES units, [14], [15], is routinely formulated as a two-stage stochastic MILP and considers ES units as stationary resources. In these tools, the first stage optimizes the ES locations and sizes, while the second stage fixes the first-stage decisions and co-optimizes the operation of existing resources and newly installed ES units. If the ES units were mobile, the complexity of the planning tool would increase. First, the ES mobility implies that the ES location is not fixed in the second stage and needs to be optimized (so-called recourse decisions). Second, the recourse decision on each mobile ES unit is binary, where it attains the value of 1 if that unit needs to be moved, or 0 if it stays. The two-stage stochastic mixed-integer problems with binary recourse decisions are more computationally demanding, and often existing solution strategies, *e.g.*, Benders' decomposition, perform poorly when applied to such problems [16].

This computational complexity can be overcome by using the progressive hedging (PH) algorithm [17], [18]. Recently, the PH algorithm has gained attention in the context of a two-stage stochastic unit commitment problem [19]. Unlike Benders' decomposition, the PH algorithm does not exploit the two-stage structure of the underlying optimization and does not separate the first- and second-stage decisions. Instead, the PH algorithm partitions the original problem in a scenario-based fashion and the first- and second-stage decisions are optimized for each scenario independently. In each scenario-based problem, the relaxation of the first-stage decision is penalized with an exogenous penalty coefficient. The algorithm iterates until the first-stage decisions across all scenarios converge with a given tolerance. The scenario-based decomposition used in the PH algorithm is shown to be an effective solution strategy for two-stage stochastic mixed-integer problems with binary recourse decisions and, therefore, it is applicable for planning tools with mobile ES units.

This paper builds on our preliminary work in [20] and makes the following contributions:

1) It takes the perspective of the DSO and formulates the optimization problem to decide on the investments in mobile ES units. The proposed optimization is a two-stage stochastic mixed-integer second order conic program (MISOCP) with binary recourse decisions, which accounts for the relocation of mobile ES units under each specific scenario. This optimization achieves the trade-off between the economic value of mobile ES units during normal operations as previously investigated in [14], [15], and [21]–[25] for different applications, and their ability to enhance distribution system resilience in case of natural disasters.
2) Operation strategy of mobile ES units is devised for both normal and emergency conditions and co-optimized throughout all time-intervals before and after the event. During the emergencies, ES units can travel among buses and form dynamic microgrids by using their spatial flexibility and optimizing the boundaries and centroids of microgrids. Transit delay of mobile ES units and switching decisions of distribution lines and loads are also formulated in the optimization model.
3) The proposed optimization is solved using the PH algorithm. The numerical results demonstrate that this method outperforms off-the-shelf solvers in terms of the computational performance. The numerical experiments also suggest that the PH performance can be improved by tuning externalities (*e.g.*, penalty coefficients).

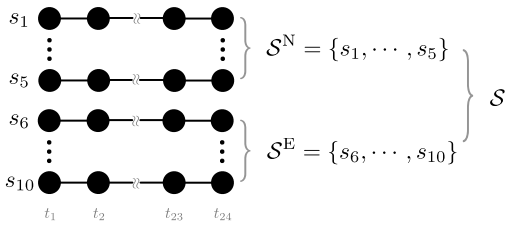

Fig. 2. A schematic representation of scenario set $\mathcal{S} = \mathcal{S}^{\mathrm{N}} \cup \mathcal{S}^{\mathrm{E}}$, which includes scenarios for normal operations in set $\mathcal{S}^{\mathrm{N}}$ and scenarios for emergency operations in $\mathcal{S}^{\mathrm{E}}$. For example, if 5 scenarios are used in each set $\mathcal{S}^{\mathrm{N}}$ and $\mathcal{S}^{\mathrm{E}}$, individual scenarios are indexed as s_1, s_2, s_3, s_4, s_5 and $s_6, s_7, s_8, s_9, s_{10}$, respectively.

The remainder of this paper is organized as follows. Section II describes the optimal operating strategies of mobile ES units during normal and emergency operations. Given these strategies, Section III presents a two-stage planning model that optimizes investments in mobile ES units. The planning model is solved using the PH algorithm as described in Section IV. Section V presents the case study that quantifies the usefulness of mobile ES units. Section VI concludes the paper.

II. Operation of Mobile ES Units

This section describes the optimal operating strategies for mobile ES units during normal and emergency operation scenarios defined by sets $\mathcal{S}^{\mathrm{N}}$ and $\mathcal{S}^{\mathrm{E}}$, both are indexed by s, that together constitute set $\mathcal{S} = \mathcal{S}^{\mathrm{N}} \cup \mathcal{S}^{\mathrm{E}}$ considered in the proposed optimization. Fig. 2 displays a relationship between scenario sets $\mathcal{S}^{\mathrm{N}}$ and $\mathcal{S}^{\mathrm{E}}$ and the numbering convention for individual scenarios. Each scenario is assigned probability ω_s such that $\sum_{s \in [\mathcal{S}^{\mathrm{N}} \cup \mathcal{S}^{\mathrm{E}}]} \omega_s = 1$ and has the number of time intervals denoted by set $\mathcal{T}$, indexed by t. The distribution system has a radial topology, which is typical for U.S. power grids, where sets $\mathcal{B}$ and $\mathcal{L}$, indexed by b and l, represent the distribution buses (nodes) and lines (edges).

A. Normal Operation

We consider the case when the DSO uses mobile ES units for performing spatio-temporal energy arbitrage during normal operations. Although the mobility of ES can be leveraged in this case, these resources are stationary during normal operations as practiced by existing utilities, see [5].

The objective function of the DSO can be formulated as:

$$\min \sum_{s\in\mathcal{S}^{\mathrm{N}}} \omega_s \cdot OC_s, \tag{1}$$

$$OC_s = \sum_{t\in\mathcal{T},b\in\mathcal{B}} C_b^{\mathrm{g}} \cdot p_{bts}^{\mathrm{g}} + \sum_{k\in\mathcal{K},b\in\mathcal{B},t\in\mathcal{T}} \left(\left| \frac{h}{100} \right| C^{\mathrm{P}}\left(p_{kbts}^{\mathrm{ch}} + p_{kbts}^{\mathrm{dis}}\right)\right), \tag{2}$$

where Eq. (1) minimizes the expected operating cost over a set of normal scenarios. Eq. (2) computes the operating cost for each scenario, which includes the generation cost of distributed generation (DG) units and ES degradation cost. The degradation cost is computed as explained in [26] and depends on charging (p_{kbts}^{ch}) and discharging (p_{kbts}^{dis}) decision variables and technology-specific degradation slope parameter h.

The DSO operations are constrained as ($\forall t \in \mathcal{T}, s \in \mathcal{S}$):

$$\left(f_{lts}^{\mathrm{p}}\right)^2 + \left(f_{lts}^{\mathrm{q}}\right)^2 \le S_l^2, \quad \forall l \in \mathcal{L}, \tag{3a}$$

$$\left(f_{lts}^{\mathrm{p}} - a_{lts}\cdot R_l\right)^2 + \left(f_{lts}^{\mathrm{q}} - a_{lts}\cdot X_l\right)^2 \le S_l^2, \quad \forall l \in \mathcal{L}, \tag{3b}$$

$$v_{s(l),t,s} - 2\left(R_l \cdot f_{lts}^{\mathrm{p}} + X_l \cdot f_{lts}^{\mathrm{q}}\right) + a_{lts}\left(R_l^2 + X_l^2\right) = v_{r(l),t,s}, \quad \forall l \in \mathcal{L}, \tag{3c}$$

$$\frac{\left(f_{lts}^{\mathrm{p}}\right)^2 + \left(f_{lts}^{\mathrm{q}}\right)^2}{a_{lts}} \le v_{s(l),t,s}, \quad \forall l \in \mathcal{L}, \tag{3d}$$

$$-\sum_{l|r(l)=0}\left(f_{lts}^{\mathrm{p}} - a_{lts}\cdot R_l\right) - p_{0,t,s}^{\mathrm{g}} + G_0 \cdot v_{0,t,s} = 0, \tag{3e}$$

$$-\sum_{l|r(l)=0}\left(f_{lts}^{\mathrm{q}} - a_{lts}\cdot X_l\right) - q_{0,t,s}^{\mathrm{g}} - B_0 \cdot v_{0,t,s} = 0, \tag{3f}$$

$$f_{bts}^{\mathrm{p}} - \sum_{l|r(l)=b}\left(f_{lts}^{\mathrm{p}} - a_{lts}\cdot R_l\right) - p_{bts}^{\mathrm{g}} + P_{bts}^{\mathrm{d}} + G_b \cdot v_{bts} - \sum_{k\in\mathcal{K}} p_{kbts}^{\mathrm{dis}} + \sum_{k\in\mathcal{K}} p_{kbts}^{\mathrm{ch}} = 0, \quad \forall b \in \mathcal{B}, \tag{3g}$$

$$f_{bts}^{\mathrm{q}} - \sum_{l|r(l)=b}\left(f_{lts}^{\mathrm{q}} - a_{lts}\cdot X_l\right) - q_{bts}^{\mathrm{g}} + Q_{bts}^{\mathrm{d}} - B_b \cdot v_{bts} - \sum_{k\in\mathcal{K}} q_{kbts}^{\mathrm{dis}} + \sum_{k\in\mathcal{K}} q_{kbts}^{\mathrm{ch}} = 0, \quad \forall b \in \mathcal{B}, \tag{3h}$$

$$\underline{P}_b^{\mathrm{g}} \le p_{bts}^{\mathrm{g}} \le \overline{P}_b^{\mathrm{g}}, \quad \forall b \in \mathcal{B}^{\mathrm{G}}, \tag{3i}$$

$$\underline{Q}_b^{\mathrm{g}} \le q_{bts}^{\mathrm{g}} \le \overline{Q}_b^{\mathrm{g}}, \quad \forall b \in \mathcal{B}^{\mathrm{G}}, \tag{3j}$$

$$\underline{V}_b \le v_{bts} \le \overline{V}_b, \quad \forall b \in \mathcal{B}. \tag{3k}$$

Equation (3c)–(3h) model a computationally tractable SOC relaxation of the ac power flows for radial networks as introduced in [27], where active and reactive power flows are f_{lts}^{p} and f_{lts}^{q} and squared magnitude of nodal voltages at sending and receiving buses of each line l are $v_{s(l)}$ and $v_{r(l)}$. This relaxation is exact for radial topologies, such as used in this paper, under rather unrestrictive assumptions, see [28] for details. In case of meshed networks, the SOC relaxation only holds under the restrictive assumption of phase shifters in strategic locations, [28]. If this assumption does not hold, other ac power flow models (*e.g.*, LinDistFlow [29]) can be used instead. The apparent power flow limit, resistance and reactance of each line are denoted by S_l, R_l and X_l. Eq. (3e)–(3f) enforce the active and reactive nodal power balance for the root bus (denoted with index 0) of the distribution system, *i.e.*, the bus that connect the distribution system to the transmission system. The active and reactive nodal power balance constraints for other distribution buses are enforced in (3g) and (3h), where P_{bts}^{d} and Q_{bts}^{d} are the active and reactive power demand. Active and reactive power injections of conventional generators are constrained in (3i) and (3j) using their minimum and maximum limits ($\underline{P}_b^{\mathrm{g}}$, $\underline{Q}_b^{\mathrm{g}}$, $\overline{P}_b^{\mathrm{g}}$, $\overline{Q}_b^{\mathrm{g}}$). The nodal voltage magnitudes are constrained within the upper ($\overline{V}_b$) and lower ($\underline{V}_b$) limits as given by (3k).

Equation (3g) and (3h) include power injections of mobile ES units (p_{kbts}^{ch} and p_{kbts}^{dis} are charging and discharging variables), which are operated as follows ($\forall k \in \mathcal{K}, t \in \mathcal{T}, s \in \mathcal{S}$):

$$e_{kts} = e_{k,t-1,s} + \sum_{b\in\mathcal{B}}\left(p_{kbts}^{\mathrm{ch}} \cdot \aleph^{\mathrm{ch}} - p_{kbts}^{\mathrm{dis}}/\aleph^{\mathrm{dis}}\right), \tag{4a}$$

$$0 \le e_{kts} \le \overline{E}_k, \tag{4b}$$

$$e_{k,t_0,s} = e_{k,t_{24},s} = 0.5\overline{E}_k, \tag{4c}$$

$$0 \le p_{kbts}^{\mathrm{ch}} \cdot \aleph^{\mathrm{ch}} \le \overline{P}_k \cdot z_{kb}, \quad \forall b \in \mathcal{B}, \tag{4d}$$

$$0 \le p_{kbts}^{\mathrm{dis}}/\aleph^{\mathrm{dis}} \le \overline{P}_k \cdot z_{kb}, \quad \forall b \in \mathcal{B}, \tag{4e}$$

$$\sum_{k\in\mathcal{K}} z_{kb} \le N_b^{\mathrm{ES}}, \quad \forall b \in \mathcal{B}, \tag{4f}$$

$$-K \cdot p_{kbts}^{\mathrm{ch}} \le q_{kbts}^{\mathrm{ch}} \le K \cdot p_{kbts}^{\mathrm{ch}}, \quad \forall b \in \mathcal{B}, \tag{4g}$$

$$-K \cdot p_{kbts}^{\mathrm{dis}} \le q_{kbts}^{\mathrm{dis}} \le K \cdot p_{kbts}^{\mathrm{dis}}, \quad \forall b \in \mathcal{B}. \tag{4h}$$

Equation (4a) relates the energy state of charge (e_{kts}) and charging and discharging decisions with imperfect, symmetric efficiencies $\aleph^{\mathrm{ch}} = \aleph^{\mathrm{dis}} < 1$. Adding Eq. (4a) makes the DSO problem in Eq. (1)–(3) temporally constrained by relating the energy state of charge for each mobile ES unit at time period t and $t-1$. Eq. (4b) limits the energy stored to $\overline{E}_k$, while the minimum level is set 0. We enforce in Eq. (4c) that the storage unit is 50% charged at the first time interval of each scenario and must remain in that state at the end of each scenario. Since buses may differ in the their ability to accommodate mobile ES units (*e.g.*, space constraints), we enforce the maximum limit on the number of mobile ES units that can be placed at each bus in Eq. (4f). Eq. (4d)–(4e) limit the maximum charging and discharging power to $\overline{P}_k$ and binary variable $z_{kb} \in \{0, 1\}$ indicates whether ES unit k is placed at but b during normal operations. If $z_{kb} = 1$, energy can be withdrawn from or injected in the ES unit; hence, z_{kb} appears in the right-hand side of Eq. (4d)–(4e). Eq. (4g) and (4h) relate the reactive power injections of mobile ES units to their charging and discharging power via parameter K that can be set by the DSO based on their techno-economic preferences (*e.g.*, to maintain a given constant power factor).

B. Emergency Operation

If a natural disaster is anticipated, the DSO prepares a resilience response plan to mitigate the damage and socio-economic losses. The response plan implies that now the DSO can exploit the mobility of mobile ES units and other resilience technologies (*e.g.*, topology switching, microgrid formation, etc). As a result, mobile ES units can be transported from their stationary locations to deal with the disaster and thus,

the emergency operation decision has a dependency on the stationary siting decision in normal operation. To optimize the route and dispatch of mobile ES units, the DSO needs to co-optimize the routing decisions with topology switching and microgrid formation as given by the model in Eq. (5)–(8).

During emergency operations, the objective function of the DSO is given by:

$$\min \sum_{s\in\mathcal{S}^{\mathrm{E}}} \omega_s \cdot EC_s, \tag{5}$$

$$EC_s = \sum_{t\in\mathcal{T},b\in\mathcal{B}} C_b^{\mathrm{g}} \cdot p_{bts}^{\mathrm{g}} + \sum_{k\in\mathcal{K},b\in\mathcal{B},t\in\mathcal{T}} \left(\left| \frac{h}{100} \right| C^{\mathrm{P}} \left(p_{kbts}^{\mathrm{ch}} + p_{kbts}^{\mathrm{dis}} \right) \right) + \sum_{k\in\mathcal{K},b\in\mathcal{B},t\in\mathcal{T}} C_b^{\mathrm{VoLL}} \left(1 - \sigma_{bts}^{\mathrm{d}} \right) p_{bts}^{\mathrm{d}}. \tag{6}$$

Note that, unlike Eq. (2), Eq. (6) includes load shedding penalized at the value of lost load (C_b^{VoLL}). The shed load is decided based on the nodal active power demand (p_{bts}^{d}) and binary decision $\sigma_{bts}^{\mathrm{d}}$. In practice, $\sigma_{bts}^{\mathrm{d}} = 0$ implies that demand at bus b and time interval t under scenario s is fully disconnected from the distribution system.

Building on the normal operation model, the distribution system in case of emergencies is modeled as ($\forall t \in \mathcal{T}, s \in \mathcal{S}^{\mathrm{E}}$):

$$\text{Equation (3c)–(3f), (3i)–(3j)}, \tag{7a}$$

$$\left(f_{lts}^{\mathrm{p}}\right)^2 + \left(f_{lts}^{\mathrm{q}}\right)^2 \le \left(\sigma_{lts}^{\mathrm{l}} S_l\right)^2, \quad \forall l \in \mathcal{L}, \tag{7b}$$

$$\left(f_{lts}^{\mathrm{p}} - a_{lts} \cdot R_l\right)^2 + \left(f_{lts}^{\mathrm{q}} - a_{lts} \cdot X_l\right)^2 \le \left(\sigma_{lts}^{\mathrm{l}} \cdot S_l\right)^2, \quad \forall l \in \mathcal{L}, \tag{7c}$$

$$f_{bts}^{\mathrm{p}} - \sum_{l|r(l)=b} \left(f_{lts}^{\mathrm{p}} - a_{lts} \cdot R_l\right) - p_{bts}^{\mathrm{g}} + \sigma_{bts}^{\mathrm{d}} \cdot P_{bts}^{\mathrm{d}} + G_b \cdot v_{bts} - \sum_{k\in\mathcal{K}} p_{kbts}^{\mathrm{dis}} + \sum_{k\in\mathcal{K}} p_{kbts}^{\mathrm{ch}} = 0, \quad \forall b \in \mathcal{B}, \tag{7d}$$

$$f_{bts}^{\mathrm{q}} - \sum_{l|r(l)=b} \left(f_{lts}^{\mathrm{q}} - a_{lts} \cdot X_l\right) - q_{bts}^{\mathrm{g}} + \sigma_{bts}^{\mathrm{d}} \cdot Q_{bts}^{\mathrm{d}} - B_b \cdot v_{bts} - \sum_{k\in\mathcal{K}} q_{kbts}^{\mathrm{dis}} + \sum_{k\in\mathcal{K}} q_{kbts}^{\mathrm{ch}} = 0, \quad \forall b \in \mathcal{B}, \tag{7e}$$

where binary line switching decision $\sigma_{lts}^{\mathrm{l}}$ is included in the right-hand side of the apparent power flow constraints in Eq. (7b)–(7c) and load shedding decision variable $\sigma_{bts}^{\mathrm{d}}$ is added to the nodal power balance constraints in Eq. (7d)–(7e).

Using the line switching decisions, the microgrid formation process is accounted for as ($\forall t \in \mathcal{T}, s \in \mathcal{S}^{\mathrm{E}}$):

$$\sum_{l\in\mathcal{L}} \sigma_{lts}^{\mathrm{l}} \ge N^{\mathrm{L}} - \max\left(N^{\mathrm{O}}, N^{\mathrm{ES}} + N^{\mathrm{DG}}\right), \tag{8a}$$

$$\sigma_{lts}^{\mathrm{l}} = 0, \ \forall l \in \mathcal{L}^{\mathrm{O}}. \tag{8b}$$

Equation (8a) ensures that the number of microgrids formed in the distribution system is consistent with the number of DGs (N^{DG}) or mobile ES units (N^{ES}) available to the DSO. Thus, if the number of outages (N^{O}) caused by the disaster is larger than the number of power sources, some parts of the distribution system will remain without any power supply. Eq. (8b) models outages of the distribution lines as given for each specific disaster scenario. Relative to [12], [13], and [30], we improve the microgrid formation process by eliminating the need in binary variables that assign a bus to a microgrid, see [31] for details. Additionally, decisions $\sigma_{lts}^{\mathrm{l}}$ can be used to change a network topology in order to improve resilience; however this aspect is beyond the scope of this study.

Since emergency operations assume mobile ES units can be transported, Eq. (4) is replaced with ($s \in \mathcal{S}^{\mathrm{E}}$):

$$\text{Equation (4a)–(4b), (4g)–(4h)}, \tag{9a}$$

$$e_{k,t_0,s} = 0.5 \cdot \overline{E}_k, \quad \forall k \in \mathcal{K}, \tag{9b}$$

$$0 \le p_{kbts}^{\mathrm{ch}} \cdot \aleph^{\mathrm{ch}} \le \overline{P}_k \cdot u_{kbts}, \quad \forall k \in \mathcal{K}, b \in \mathcal{B}, t \in \mathcal{T}, \tag{9c}$$

$$0 \le p_{kbts}^{\mathrm{dis}} / \aleph^{\mathrm{dis}} \le \overline{P}_k \cdot u_{kbts}, \quad \forall k \in \mathcal{K}, b \in \mathcal{B}, t \in \mathcal{T}, \tag{9d}$$

$$\sum_{k\in\mathcal{K}} u_{kbts} \le N_b^{\mathrm{ES}}, \quad \forall b \in \mathcal{B}, t \in \mathcal{T}, \tag{9e}$$

$$u_{kb_1ts} - u_{kb_1,t+1,s} \le 1 - u_{kb_2,t+\tau,s}, \quad \forall k \in \mathcal{K}, \ b_1 \ne b_2 \in \mathcal{B}, t \in \mathcal{T}, \tau \in \left[1, \cdots, \min\left(T_{b1,b2,t}^{\mathrm{d}}, N^{\mathrm{t}} - t\right)\right]. \tag{9f}$$

Equation (9b) limits the energy state of charge in the first time interval only, *i.e.*, there is no limit for the last time interval and the ES unit can fully be discharged, if necessary. The routing decisions on each mobile ES units are using binary variable u_{kbts} that is set to 1 if mobile ES unit k is at bus b during time interval t under scenario s. Otherwise, $u_{kbts} = 0$. In (9c)–(9d), binary variable u_{kbts} decides if mobile ES units can be charged or discharged. In other words, the role of u_{kbts} in (9d)–(9c) is similar to z_{kb} in (4d)–(4e), but ensures that the mobile ES units can move between different buses. The limit on the maximum number of ES units that can be simultaneously connected to each bus is enforced in Eq. (9e). Eq. (9f) models the transition delay on moving mobile ES unit from bus $b_1 \in \mathcal{B}$ to bus $b_2 \in \mathcal{B}$, where $T_{b_1,b_2,t}^{\mathrm{d}}$ is a given transition time between buses b_1 and b_2. Similarly to Eq. (4a), Eq. (9f) makes the resulting optimization problem temporally constrained as it relates decisions u_{kbts} and $u_{kb,t+1,s}$. In practice, the value of $T_{b_1,b_2,t}^{\mathrm{d}}$ can be determined based on the availability and length of transportation routes. Note that (9f) is structurally equivalent to minimum up and down time constraints on the on/off status of conventional generators modeled in UC problems [19].

III. Planning With Mobile ES Units

Using the operating models for normal and emergency operation in Section II, this section builds a planning model that optimizes investment decisions on mobile ES units. The planning model is schematically shown in Fig. 3 with interfaces between the planning and operating decisions, as well as the decisions made during normal and emergency operations. The objective of this optimization is to allocate the mobile ES units in such a way that these units are operated as stationary resources during the normal operations and can be transported to other locations, or among multiple other locations, in case of natural disasters.

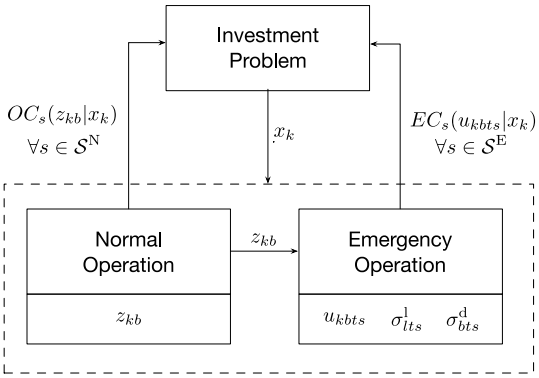

Fig. 3. Structure of the proposed planning problem with mobile ES units and interfaces between the planning and operating decisions.

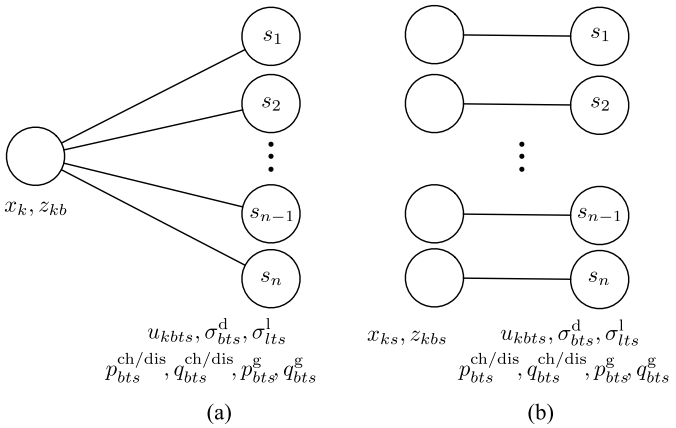

Fig. 4. Comparison of the (a) original problem and (b) PH decomposed subproblems.

The planning problem is given as follows:

$$\min \Bigg[\gamma \cdot IC(x_k) + \sum_{s \in \mathcal{S}^{\mathrm{N}}} \omega_s \cdot OC_s(z_{kb}|x_k) + \sum_{s \in \mathcal{S}^{\mathrm{E}}} \omega_s \cdot EC_s(u_{kbts}|x_k) \Bigg], \tag{10a}$$

$$IC(x_k) = \sum_{k \in \mathcal{K}} \left(C^{\mathrm{P}} \cdot \overline{P}_k + C^{\mathrm{E}} \cdot \overline{E}_k \right) \cdot x_k \tag{10b}$$

$$\sum_{b \in \mathcal{B}} z_{kb} \leq x_k, \quad \forall k \in \mathcal{K}, \tag{10c}$$

$$\sum_{b \in \mathcal{B}} u_{kbts} \leq x_k, \quad \forall k \in \mathcal{K}, t \in \mathcal{T}, s \in \mathcal{S}^{\mathrm{E}}, \tag{10d}$$

$$u_{kb,t_0,s} = z_{kb}, \quad \forall k \in \mathcal{K}, b \in \mathcal{B}, s \in \mathcal{S}^{\mathrm{E}}, \tag{10e}$$

$$\text{Eq. (2)– (4)}, \quad \forall s \in \mathcal{S}^{\mathrm{N}}, \tag{10f}$$

$$\text{Eq. (6)– (8)}, \quad \forall s \in \mathcal{S}^{\mathrm{E}}. \tag{10g}$$

Equation (10a) minimizes the sum of the three terms. The first term is the investment cost of mobile ES units, where parameter γ is a capital recovery factor that prorates the investment cost on a daily basis using the net present value approach, [14]. The second and third terms represent the expected operating cost during normal and emergency operations as computed in Eq. (2) and Eq. (6), respectively. Eq. (10b) computes the investment cost of installing mobile ES unit k based on its power and energy ratings $\overline{P}_k$ and $\overline{E}_k$ priced at C^{P} and C^{E}, respectively, as previously used in [14] and [15]. The installation decision is modeled by binary variable $x_k \in \{0, 1\}$. If $x_k = 1$, mobile ES unit k is installed, otherwise $x_k = 0$. Eq. (10c) and (10d) relate z_{kb} and u_{kbts} to the respective investment decision (x_k). If $x_k = 0$, it follows from (10c) and (10d) that no storage can be used during normal and emergency operations. On the other hand, if $x_k = 1$, z_{kb} is optimized for all scenarios $s \in \mathcal{S}^{\mathrm{N}}$ and u_{kbts} is optimized for each scenario $s \in \mathcal{S}^{\mathrm{E}}$. Eq. (10e) ensures that each mobile ES unit is routed to its temporary locations during emergencies from its stationary locations during normal operations. Eq. (10f) and (10g) impose constraints for the normal and emergenecy operations as explained in Section II.

As shown in Fig. 3, $OC_s(z_{kb}|x_k)$ and $EC_s(u_{kbts}|x_k)$ depend on binary variables x_k, z_{kb} and u_{kbts}. Binary decisions x_k constrain the placement of mobile ES units (z_{kb}) during normal operations and their routing decisions during emergency operations (u_{kbts}). Furthermore, the binary routing decisions (u_{kbts}) also depend on the binary placement decisions (z_{kb}) as in Eq. (10e). This dependency makes the planning problem in Eq. (10) a two-stage MISOCP with binary recourse decisions.

TABLE II
COMPLEXITY OF THE ORIGINAL AND DECOMPOSED PROBLEMS

	Original problem	Decomposed subproblem
Binary variables	$u_{kbts}, \sigma^{\mathrm{d}}_{bts}, \sigma^{\mathrm{l}}_{lts}$ z_{kb}, x_k	$u_{kbt}, \sigma^{\mathrm{d}}_{bt}, \sigma^{\mathrm{l}}_{lt}$ z_{kb}, x_k
# of binary variables	$N^{\mathrm{S}}N^{\mathrm{T}}[N^{\mathrm{ES}}(N^{\mathrm{B}}+1)+N^{\mathrm{L}}]$ $+N^{\mathrm{ES}}(N^{\mathrm{B}}+1)$	$N^{\mathrm{T}}[N^{\mathrm{ES}}(N^{\mathrm{B}}+1)+N^{\mathrm{L}}]$ $+N^{\mathrm{ES}}(N^{\mathrm{B}}+1)$
Continuous variables	$p^{\mathrm{ch/dis}}_{kbts}, q^{\mathrm{ch/dis}}_{kbts}$ $p^{\mathrm{g}}_{bts}, q^{\mathrm{g}}_{bts}$	$p^{\mathrm{ch/dis}}_{kbt}, q^{\mathrm{ch/dis}}_{kbt}$ $p^{\mathrm{g}}_{bt}, q^{\mathrm{g}}_{bt}$
# of continuous variables	$4N^{\mathrm{S}}N^{\mathrm{T}}N^{\mathrm{ES}}N^{\mathrm{B}}$ $+2N^{\mathrm{S}}N^{\mathrm{T}}N^{\mathrm{B}}$	$4N^{\mathrm{T}}N^{\mathrm{ES}}N^{\mathrm{B}}$ $+2N^{\mathrm{T}}N^{\mathrm{B}}$

IV. SOLUTION TECHNIQUE

The proposed two-stage stochastic MISOCP in Eq. (10) is computationally demanding due to the co-optimization of investment decisions for normal and contingency operations, binary recourse decisions, and multi-period optimization within each scenario considered. Off-the-shelf solvers can be used to solve the model, but their performance is limited for large networks or instances with a large number of scenarios. To solve this problem efficiently, we apply the PH algorithm [18] to the proposed planning problem. As shown in Fig. 4, the PH algorithm decomposes the original problem in (10) into $N^{\mathrm{S}} = card(\mathcal{S})$ subproblems. The decomposition exploits the notion that the investment decisions (x_k) and the mobile ES placement (z_{kb}) are common for all scenarios and that the routing decisions (u_{kbts}) can be optimized for each scenario individually. Accordingly, the decomposition yields N^{S} subproblems, where the integrality condition on x_k and z_{kb} is relaxed. Since each subproblem has significantly fewer binary decision variables than the original planning problem, it is computationally more tractable. Furthermore, all subproblems can be solved in parallel, which further accelerates computing performance. We compare the number of variables for

Algorithm 1 PH Algorithm for Installing Mobile ES Units

Step 1. $i := 0, m_s^{(i=0)} := 0, w_s^{(i=0)} := 0$

Step 2. **for** $s \leftarrow 1$ **to** N^{S} **do**

$z_{kbs}^{(i=0)}, x_{ks}^{(i=0)} \leftarrow \arg\min_{z,x} \gamma \cdot IC + OC_s + EC_s$

end

$\bar{z} \leftarrow \sum_{s\in\mathcal{S}} \omega_s \cdot z_{kbs}^{(i=0)}, \ \bar{x} \leftarrow \sum_{s\in\mathcal{S}} \omega_s \cdot x_{ks}^{(i=0)}$

Step 3. **do**

$i \leftarrow i+1$

for $s \leftarrow 1$ **to** N^{S} **do**

$m_s^{(i)} \leftarrow m_s^{(i-1)} + \rho_z \cdot \left(z_{kb}^{(i-1)} - \bar{z}\right)$

$w_s^{(i)} \leftarrow w_s^{(i-1)} + \rho_x \cdot \left(x_k^{(i-1)} - \bar{x}\right)$

$z_{kbs}^{(i)}, \ x_{ks}^{(i)} \leftarrow \arg\min_{z,x} \gamma \cdot IC + OC_s + EC_s + m_s^{(i)} \cdot z_{kb} + \frac{\rho_z}{2}\|z_{kb} - \bar{z}\|^2 + w_s^{(i)} \cdot x_k + \frac{\rho_x}{2}\|x_k - \bar{x}\|^2$

end

$\bar{z} \leftarrow \sum_{s\in\mathcal{S}} \omega_s \cdot z_{kbs}^{(i)}, \ \bar{x} \leftarrow \sum_{s\in\mathcal{S}} \omega_s \cdot x_{ks}^{(i)}$

$g^{(i)} \leftarrow \sum_{s\in\mathcal{S}} \omega_s \cdot \left\|z_{kbs}^{(i)} - \bar{z}\right\| + \sum_{s\in\mathcal{S}} \omega_s \cdot \left\|x_{ks}^{(i)} - \bar{x}\right\|$

while convergence: $g^{(i)} < \epsilon$

return $z_{kbs}^{(i)}$

the original and each subproblem in Table II and note that the advantage of the decomposition increases as N^{S} increases. When all subproblems are solved, decisions x_k and z_{kb} can be recovered based on their relaxed values for each subproblem. The algorithm continues until convergence. The recovered values are x_k and z_{kb} respect constraints imposed by each scenario and their multi-temporal dynamics.

The PH algorithm is implemented as explained in Algorithm 1 and further detailed below:

- *Step 1*: The PH algorithm is initialized by setting the iteration counter $i = 0$ and multipliers $m_s^{(i=0)} = w_s^{(i=0)} = 0$.
- *Step 2*: Each of N^{S} subproblems is solved in parallel to obtain binary decisions $z_{kb}^{(i=0)}$ and $x_k^{(i=0)}$. When all subproblems are solved, we compute $\bar{z}$ and $\bar{x}$ as the weighted average of all subproblem solutions.
- *Step 3*: The iteration counter is updated, *i.e.*, $i := i+1$. For each subproblem we update the value of PH multipliers $m_s^{(i)}$ and $w_s^{(i)}$ using the values of $z_{kb}^{(i-1)}$ and $x_k^{(i-1)}$. Then each relaxed subproblem is solved to obtain $z_{kbs}^{(i)}$ and $x_{ks}^{(i)}$, where the deviations of $z_{kb}^{(i)}$ from $\bar{z}$ and $x_k^{(i)}$ from $\bar{x}$ are penalized using exogenous penalty coefficients ρ_z and ρ_x. After all subproblems are solved, we use $z_{kbs}^{(i)}$ and $x_{ks}^{(i)}$ to update the values of $\bar{z}$ and $\bar{x}$. The iterative process continues until the mismatch $g^{(i)}$ is less than a given tolerance ϵ.

The convergence of Algorithm 1 is accelerated by setting penalty coefficients ρ_x and ρ_z based on the cost coefficients of relaxed variables x_k and z_{kb}:

$$\rho_x = \frac{\gamma \cdot IC}{x_{\max}^{(i=0)} - x_{\min}^{(i=0)} + 1}, \tag{11a}$$

TABLE III
INVESTMENT DECISIONS ON MOBILE ES UNITS

Line Outage	no outage	line 6	line 5	line 4	line 13
Potential Load Shedding	0kW	21.9kW (bus 6)	51kW (bus 5-6)	101kW (bus 4-6)	152kW (bus 13-14)
N^{ES} installed	0	1	1	2	2
ES capacity	0MWh	1MWh	1MWh	2MWh	2MWh
Initial ES bus	-	2	5	1 and 12	0 and 12

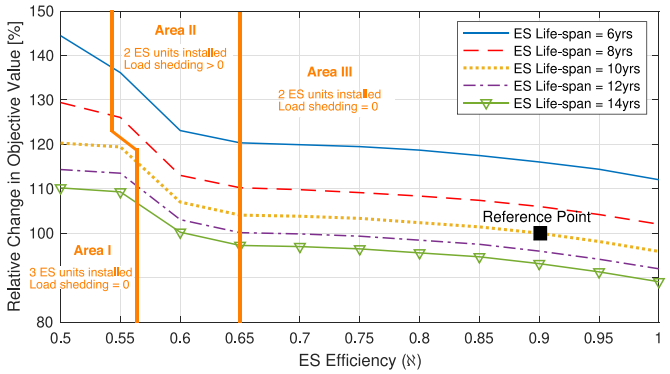

Fig. 5. Effect of the ES lifetime and the symmetric charging and discharging efficiency ($\aleph^{\mathrm{dis}} = \aleph^{\mathrm{dis}} = \aleph$) on the objective function value. The reference point is obtained for the base case parameters.

$$\rho_z = \frac{\gamma \cdot IC}{z_{\max}^{(i=0)} - z_{\min}^{(i=0)} + 1}. \tag{11b}$$

Equation (11) is a generalization of the cost proportional method in [18], which exploits the fact that the PH algorithm is best-performing when the penalty value is a multiple of unit cost in the objective function. The PH implementation in Algorithm 1 also extends the use of penalty factors to two binary variables x_k and z_{kb} that are relaxed by the algorithm.

V. CASE STUDIES

We use the 15-bus radial distribution test system described in [32] with one DG located at bus 11. The system diagram is given in Fig. 6–(a). The mobile ES units considered for installation have $\overline{E}_k$=1MWh, $\overline{P}_k$=0.15MW, $\aleph^{\mathrm{ch}}$=$\aleph^{\mathrm{dis}}$ = 0.9, C^{P}=\$1,000/kW and C^{E}=\$50/kWh [14] and the expected lifetime is 10 years. These nameplate parameters for mobile ES units are generally consistent with technical specifications of the demonstration units used by Consolidated Edison of New York, [5], and can be scaled to accommodate other ES technologies. The transition time enforced in Eq. (9f) is defined as $T^{\mathrm{d}}_{b_1,b_2,t} = \min(|b_1 - b_2|, d_{b_1,b_2})$ and d_{b_1,b_2} is generated by using the shortest path algorithm where d_{b_1,b_2} is the number of lines between buses b_1 and b_2. For instance, the transition time between bus 0 and 14 in Fig. 6 is set as $T^{\mathrm{d}}_{0,14,t} = \min(|0-14|, d_{0,14}) = \min(14, 3) = 3$. The value of lost load is C_b^{VoLL} = \$5,000/MWh. All simulations have been carried out using Gurobi solver v7.5 on Julia 0.6.2/JuMP 0.17 [33] on an Intel Xeon 2.6 GHz processor with 20 Cores and 40GB memory. The MIP gap is set 0.1%. Our code and input data can be downloaded in [34].

TABLE IV
OPTIMAL ROUTING DECISIONS AND STATE-OF-CHARGE FOR THE MOBILE ES UNIT DURING EMERGENCY SCENARIOS

		Time interval #																							
		1	2	3	4	5	6	7	8	9	10	11	12	13	14	15	16	17	18	19	20	21	22	23	24
Bus #	s_6	0	0	0	0	T	1	1	1	1	1	T	0	0	0	0	0	T	1	1	1	1	1	1	1
	s_7	0	0	0	0	T	1	1	1	1	1	T	0	0	0	0	0	T	1	1	1	1	1	1	1
	s_8	0	0	0	0	T	12	12	12	12	12	T	0	0	0	0	0	T	12	12	12	12	12	12	12
	s_9	0	T	12	12	T	13	13	13	13	13	13	T	12	12	12	12	12	T	13	13	13	13	13	13
	s_{10}	0	T	1	1	T	T	3	3	3	3	3	T	2	2	2	2	2	T	3	3	3	3	3	3
e_{kts}, MWh	s_6	0.5	0.65	0.8	0.95	T	0.81	0.66	0.53	0.4	0.26	T	0.38	0.53	0.68	0.83	0.98	T	0.84	0.7	0.56	0.42	0.28	0.14	0
	s_7	0.52	0.67	0.82	0.97	T	0.82	0.67	0.53	0.38	0.24	T	0.39	0.54	0.69	0.84	0.99	T	0.85	0.71	0.57	0.43	0.29	0.14	0
	s_8	0.5	0.65	0.8	0.95	T	0.81	0.67	0.54	0.4	0.27	T	0.38	0.53	0.68	0.83	0.98	T	0.84	0.7	0.56	0.42	0.28	0.15	0
	s_9	0.61	T	0.76	0.91	T	0.77	0.62	0.49	0.36	0.23	0.09	T	0.24	0.39	0.54	0.69	0.84	T	0.7	0.56	0.42	0.28	0.15	0
	s_{10}	0.58	T	0.73	0.88	T	T	0.73	0.59	0.44	0.29	0.14	T	0.29	0.44	0.59	0.74	0.89	T	0.74	0.59	0.44	0.29	0.14	0

Labels 'T' defines that the mobile ES unit is in transit.

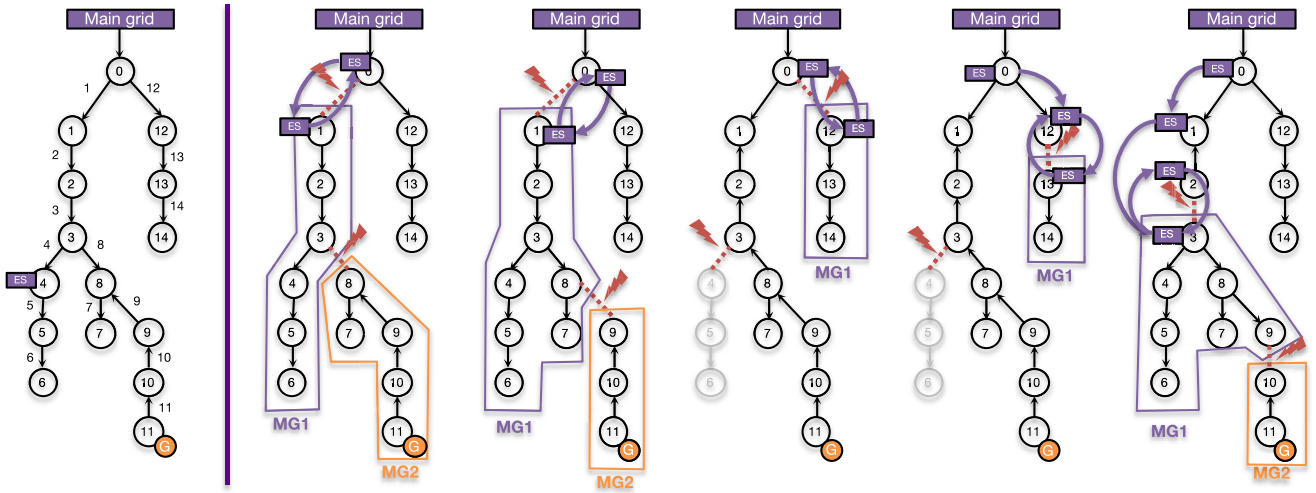

(a) Benchmark case: Stationary ES (b) Emergency scenario s_6 (c) Emergency scenario s_7 (d) Emergency scenario s_8 (e) Emergency scenario s_9 (f) Emergency scenario s_{10}

Fig. 6. Placement of the (a) stationary ES unit and (b-f) mobile ES units with optimal routing directions during emergency scenarios ($s_6 - s_{10}$). Plot (a) also denotes the line indices. Plots (b-f) includes the bounds of the microgrids (MGs) formed by the mobile ES unit and DG. Note that the mobile ES unit is placed at bus 0 during normal operations in plots (b-f). The block 'Main grid' refers to the rest of the power system connected to the distribution system considered in this case study.

A. Case Study 1: Investments in Mobile ES Units

The problem in Eq. (10) is solved with one normal and one emergency scenarios, *i.e.*, $N^S = 2$. Probabilities for the scenarios are artificially generated as $\sum_{s\in\mathcal{S}^{\mathrm{N}}} \omega_s = 0.9$ and $\sum_{s\in\mathcal{S}^{\mathrm{E}}} \omega_s = 0.1$. In each case, the emergency scenario is modeled by an outage of line 4, 5, 6, or 13 at time interval $t = 6$ hour. Each outage leads to a different potential load shedding amount, thus representing a different level of severity for the DSO. The resulting investment decisions are given in Table III. First, no mobile ES units are installed in the case without outages, *i.e.*, operating ES units as a stationary resource for normal operations does not create sufficient value to the distribution system to economically justify their installation. On the other hand, as the potential load shedding increases from 21.9 kW to 152 kW for each of the four outages, the need in mobile ES units increases and thus larger capacity is installed. After installing and using mobiles ES units, no load shedding occurs in all four outages. Thus, exploiting mobility of ES units during emergencies yields a sufficient added value for their installation and use during both normal and emergency operations. The shift in installation decisions among four outages is primarily driven by the prevented load shedding, *i.e.*, more severe outages require more ES capacity.

Fig. 5 displays the effect of the ES lifetime and the symmetric charging and discharging efficiency ($\aleph^{\mathrm{ch}} = \aleph^{\mathrm{dis}} = \aleph$) on the value of the objective function for the outage on line 4 as given in Table III. The value of the objective function in Eq. (10a) reduces monotonically as the efficiency of ES units increases regardless of the lifetime period considered. Similarly, the longer lifetime period the lower value is attained in the objective function. This is due to the fact that more efficient and longer serving ES units reduce the investment cost, while providing greater benefit to the system.

Accordingly, the curves in Fig. 5 have multiple areas, where each area is differentiated by the number of mobile ES units installed and the amount of load shedding. In Area I of Fig. 5, three mobile ES units are needed to fully prevent load shedding. However, as the efficiency of mobile ES units increases, less units are installed. The breaking point between Area II and Area III occurs at $\aleph^{\mathrm{ch}} = \aleph^{\mathrm{dis}} = 0.65$. The difference in these two areas is in the amount of load shedding. If $\aleph^{\mathrm{ch}} = \aleph^{\mathrm{dis}} \leq 0.65$, the physical capacity of two mobile ES

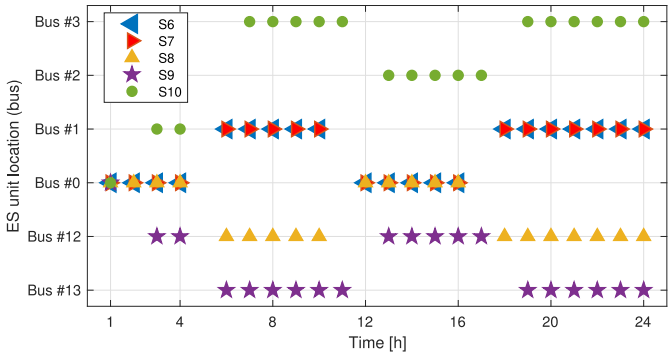

Fig. 7. Optimal routing decisions of the mobile ES unit for each emergency scenario ($s_6 - s_{10}$).

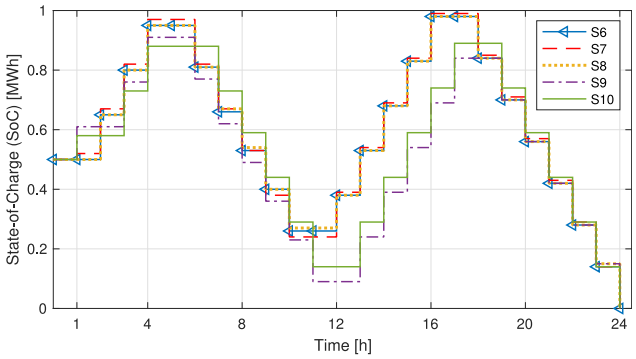

Fig. 8. State-of-charge of the mobile ES unit (variable e_{kbts}) for each emergency scenario ($s_6 - s_{10}$).

TABLE V
EFFECTS OF THE ES MOBILITY ON LOAD SHEDDING

	Lost Load, MWh					Average Lost Load, MWh	Objective Value, $
	s_6	s_7	s_8	s_9	s_{10}		
Without ES	4.40	5.19	6.73	4.45	3.31	4.82	2877.20
Stationary ES	3.29	4.07	5.64	3.35	2.18	3.71	2393.99
Mobile ES	2.91	3.65	5.23	2.95	1.84	3.32	2200.05

units is not sufficient to fully prevent load shedding and the residual load shedding is not sufficient to economically justify installing the third unit. However, as the efficiency improves and $\aleph^{\text{ch}} = \aleph^{\text{dis}} > 0.65$, two mobiles ES units become sufficient to fully prevent load shedding. Notably, the effect of the ES lifetime is most evident for ES units with a lower efficiency, where it can increase the number of ES units needed (*e.g.*, three instead of two units as with $\aleph^{\text{ch}} = \aleph^{\text{dis}} \approx 0.55$.)

B. Case Study 2: Effectiveness of the ES Mobility

This case study considers five normal and five emergency scenarios (each emergency starts at time interval $t = 6$ hour), *i.e.*, $N^S = 10$, and compares three cases. The probability set for the scenarios is generated in the same way as Case Study 1. The first case assumes that there is no ES installed, *i.e.*, $x_k = 0$. The second case assumes that the ES is a stationary resource and cannot move at any time, *i.e.*, $z_{kb} = u_{kbts}, \forall t \in \mathcal{T}$. This case is consistent with the traditional ES investment problems in [14] and [15]. The third case stands for the proposed problem in (10) and demonstrates the full range of benefits attained with mobile ES units and microgrid formation.

The cases with stationary and mobile ES units are compared in Fig. 6, which illustrates the ES placement at bus number 0 during normal operations ($s_1 - s_5$) and illustrates the routing directions of the single ES unit installed for each emergency scenario ($s_6 - s_{10}$). Additionally, Table IV itemizes the mobile ES location and its energy state of charge under each emergency scenario; these results are also visualized in Fig. 7 and Fig. 8. Between these two cases, the ES placement decisions during normal operations differ. The stationary ES unit is installed at bus 4 during normal operations and cannot change its location for emergencies, as shown in Fig. 6-(a). As a result, of this placement decisions, the stationary ES unit can only provide back up support and form a microgrid for upstream outages. For example, in case of outages of lines 5, 8, or 12, the stationary ES unit at bus 4 will not be able to provide back up power supply. On the other hand, the mobile ES unit is installed at bus 0 during normal operations, see Fig. 6-(b)-(f). From this location, the mobile ES unit can be routed to a different location as necessitated by the needs of each individual emergency scenario and form a microgrid using line and load switches. In these results, the optimization routes mobile ES units among closely located buses since it requires less transition time, as modeled by Eq. (9f), and increases the ES usage for reducing load shedding. Furthermore, the routing decision on mobile ES unit are co-optimized with the DG at bus 11 to improve distribution system performance. Thus, two microgrids are formed under emergency scenarios in Fig. 6-(b),(c),(f), where one is sourced by the mobile ES unit transported from bus 0, where it is located during normal operations, and the other one is sourced by the DG located at bus 11. On the other hand, the emergency scenarios in Fig. 6-(d), (e) lead to load shedding at buses 4-6 since the installation of the second ES unit is not economically justified and there is no DG available.

Since the capacity of the mobile ES unit is limited, it occasionally needs to replenish the stored energy and therefore commutes between the microgrid location and the unaffected part of the distribution system. For example, as shown in Table IV for emergency scenario (s_6), the mobile ES unit travels between bus 0 and bus 1 four times during the course of the optimization horizon. All emergency scenarios have unique routing decisions, which differ based on the severity of each emergency scenario. This difference emphasizes the usefulness of mobile ES units in accommodating unique features of specific emergency scenarios.

Table V compares the three cases considered in terms of the total load shedding and objective value. First, using mobile ES units reduces the total lost load (computed as $\sum_{b\in\mathcal{B}}\sum_{t\in\mathcal{T}}(1-\sigma^{\text{d}}_{bts})p^{\text{d}}_{bts}$) across all considered emergency scenarios relative to the other two cases. Thus, the average load shedding is reduced by 10.52% compared to the case with stationary ES units due to the mobility of ES units. Second, the case with mobile ES units returns the least-cost objective function value among all three cases.

TABLE VI
PERFORMANCE OF THE BF AND PH IMPLEMENTATIONS

# of scenarios	Objective value, $		CPU time, s	
	BF	PH	BF	PH
2	1,930.3	1,966.2	1,193	7,686
4	N/A	2,165.2	N/A	8,912
6	N/A	2,513.6	N/A	10,695
8	N/A	2,376.3	N/A	8,067
10	N/A	2,200.1	N/A	10,912
20	N/A	2,265.3	N/A	10,066
40	N/A	1,891.8	N/A	18,218
60	N/A	1,874.0	N/A	12,456

TABLE VII
COMPUTATION TIME [S] OF PH IMPLEMENTATIONS - 37 AND 123 BUS SYSTEMS

# of scenarios	20	40	60
IEEE 37-bus system	11,964	16,511	13,411
IEEE 123-bus system	17,345	14,008	16,301

C. Computational Performance

Table VI compares the proposed PH implementation and the brute-force (BF) implementation (*i.e.*, solving the proposed optimization directly using the Gurobi solver) in terms of their computational performance and optimality with a different number of scenarios. The BF approach is only able to solve the case with two scenarios, and it is 6x times faster while the objective functions and the investment decision on mobile ES units are nearly identical to that of the PH implementation. The BF becomes incapable of completing the task within the time limit (12 hours) for more than two scenarios. The PH implementation, on the other hand, returns the optimal solution within 8 hours for all cases. To assess computational scalability of the proposed model and PH implementation to larger networks, we carry out experiments on the IEEE 37- and 123-bus systems, [35]. Table VII demonstrates CPU times for these simulations. As expected, the CPU times monotonically increase for larger networks. On the other hand, the effect of increasing the number of scenarios is not monotonic, similarly to the results in Table VI. This effect is due to paralleling subproblems computation, which enables the PH implementation to have roughly the same amount of CPU time regardless of the number of scenarios. This implies that using parallel computations allows for accommodating an even larger number of scenarios without further computational complexity.

VI. CONCLUSION

This paper describes an approach to optimize investments of the DSO in mobile ES units. The ability of mobile ES units to move between different locations is used to trade-off the least-cost operations during normal operations and the need to enhance power grid resilience in case of natural disasters. The proposed optimization is a two-stage stochastic MISOCP with binary recourse decisions, which account for the relocation of mobile ES units under specific disaster scenarios. The proposed optimization is solved using the PH algorithm. The numerical experiments reveal that the mobile ES reduce the operating costs and the total amount of load shedding caused by natural disasters relative to the cases without ES units or with stationary ES units.

REFERENCES

[1] J.-P. Watson *et al.*, "Conceptual framework for developing resilience metrics for the electricity, oil, and gas sectors in the united states," Sandia Nat. Lab., Albuquerque, NM, USA, Rep. SAND2014-18019, 2014.

[2] S. Neumayer and E. Modiano, "Assessing the effect of geographically correlated failures on interconnected power-communication networks," in *Proc. IEEE Int. Conf. Smart Grid Commun.*, 2013, pp. 366–371.

[3] E. Vugrin, A. Castillo, and C. Silva-Monroy, "Resilience metrics for the electric power system: A performance-based approach," Sandia Nat. Lab., Albuquerque, NM, USA, Rep. SAND-2017-1493, 2017.

[4] G. Huang, J. Wang, C. Chen, J. Qi, and C. Guo, "Integration of preventive and emergency responses for power grid resilience enhancement," *IEEE Trans. Power Syst.*, vol. 32, no. 6, pp. 4451–4463, Nov. 2017.

[5] *Con Edison Developing Energy Storage System on Wheels*. Accessed: Mar. 1, 2018. [Online]. Available: https://www.coned.com/en/about-con-edison/media/news/20160712/energy-storage-on-wheels

[6] Y. Wang, C. Chen, J. Wang, and R. Baldick, "Research on resilience of power systems under natural disasters—A review," *IEEE Trans. Power Syst.*, vol. 31, no. 2, pp. 1604–1613, Mar. 2016.

[7] E. Rappaport *et al.*, "Advances at the national hurricane center," *Weather Forecast.*, vol. 24, no. 2, pp. 395–419, 2009.

[8] C. Wang, Y. Hou, F. Qiu, S. Lei, and K. Liu, "Resilience enhancement with sequentially proactive operation strategies," *IEEE Trans. Power Syst.*, vol. 32, no. 4, pp. 2847–2857, Jul. 2017.

[9] B. Zhang, P. Dehghanian, and M. Kezunovic, "Optimal allocation of PV generation and battery storage for enhanced resilience," *IEEE Trans. Smart Grid*, to be published.

[10] M. E. Nassar and M. M. A. Salama, "Adaptive self-adequate microgrids using dynamic boundaries," *IEEE Trans. Smart Grid*, vol. 7, no. 1, pp. 105–113, Jan. 2016.

[11] Z. Wang and J. Wang, "Self-healing resilient distribution systems based on sectionalization into microgrids," *IEEE Trans. Power Syst.*, vol. 30, no. 6, pp. 3139–3149, Nov. 2015.

[12] S. Lei, J. Wang, C. Chen, and Y. Hou, "Mobile emergency generator pre-positioning and real-time allocation for resilient response to natural disasters," *IEEE Trans. Smart Grid*, vol. 9, no. 3, pp. 2030–2041, May 2018.

[13] K. S. A. Sedzro, A. J. Lamadrid, and L. F. Zuluaga, "Allocation of resources using a microgrid formation approach for resilient electric grids," *IEEE Trans. Power Syst.*, vol. 33, no. 3, pp. 2633–2643, May 2018.

[14] H. Pandžić, Y. Wang, T. Qiu, Y. Dvorkin, and D. S. Kirschen, "Near-optimal method for siting and sizing of distributed storage in a transmission network," *IEEE Trans. Power Syst.*, vol. 30, no. 5, pp. 2288–2300, Sep. 2015.

[15] R. Fernández-Blanco, Y. Dvorkin, B. Xu, Y. Wang, and D. S. Kirschen, "Optimal energy storage siting and sizing: A WECC case study," *IEEE Trans. Sustain. Energy*, vol. 8, no. 2, pp. 733–743, Apr. 2017.

[16] H. D. Sherali and X. Zhu, *Two-Stage Stochastic Mixed-Integer Programs: Algorithms and Insights*. Boston, MA, USA: Springer, 2009, pp. 405–435.

[17] R. T. Rockafellar and R. J.-B. Wets, "Scenarios and policy aggregation in optimization under uncertainty," *Math. Oper. Res.*, vol. 16, no. 1, pp. 119–147, 1991.

[18] J.-P. Watson and D. L. Woodruff, "Progressive hedging innovations for a class of stochastic mixed-integer resource allocation problems," *Comput. Manag. Sci.*, vol. 8, no. 4, pp. 355–370, 2011.

[19] S. M. Ryan, R. J.-B. Wets, D. L. Woodruff, C. Silva-Monroy, and J.-P. Watson, "Toward scalable, parallel progressive hedging for stochastic unit commitment," in *Proc. IEEE Power Energy Soc. Gen. Meeting (PES)* 2013, pp. 1–5.

[20] J. Kim and Y. Dvorkin, "Enhancing distribution resilience with mobile energy storage: A progressive hedging approach," in *Proc. IEEE Power Energy Soc. Gen. Meeting (PES)*, 2018, pp. 1–5. [Online]. Available: https://arxiv.org/abs/1803.01184

[21] B. Xu *et al.*, "Scalable planning for energy storage in energy and reserve markets," *IEEE Trans. Power Syst.*, vol. 32, no. 6, pp. 4515–4527, Nov. 2017.

[22] Y. Dvorkin *et al.*, "Co-planning of investments in transmission and merchant energy storage," *IEEE Trans. Power Syst.*, vol. 33, no. 1, pp. 245–256, Jan. 2018.

[23] M. Carrión, Y. Dvorkin, and H. Pandžić, "Primary frequency response in capacity expansion with energy storage," *IEEE Trans. Power Syst.*, vol. 33, no. 2, pp. 1824–1835, Mar. 2018.
[24] Y. Dvorkin, "Can merchant demand response affect investments in merchant energy storage?" *IEEE Trans. Power Syst.*, vol. 33, no. 3, pp. 2671–2683, May 2018.
[25] A. Hassan and Y. Dvorkin, "Energy storage siting and sizing in coordinated distribution and transmission systems," *IEEE Trans. Sustain. Energy*, vol. 9, no. 4, pp. 1692–1701, Oct. 2018.
[26] M. A. Ortega-Vazquez, "Optimal scheduling of electric vehicle charging and vehicle-to-grid services at household level including battery degradation and price uncertainty," *IET Gener. Transm. Distrib.*, vol. 8, no. 6, pp. 1007–1016, Jun. 2014.
[27] M. Farivar and S. H. Low, "Branch flow model: Relaxations and convexification—Part I," *IEEE Trans. Power Syst.*, vol. 28, no. 3, pp. 2554–2564, Aug. 2013.
[28] S. H. Low, "Convex relaxation of optimal power flow—Part II: Exactness," *IEEE Trans. Control Netw. Syst.*, vol. 1, no. 2, pp. 177–189, Jun. 2014.
[29] M. E. Baran and F. F. Wu, "Network reconfiguration in distribution systems for loss reduction and load balancing," *IEEE Trans. Power Del.*, vol. 4, no. 2, pp. 1401–1407, Apr. 1989.
[30] C. Chen, J. Wang, F. Qiu, and D. Zhao, "Resilient distribution system by microgrids formation after natural disasters," *IEEE Trans. Smart Grid*, vol. 7, no. 2, pp. 958–966, Mar. 2016.
[31] T. Ding, Y. Lin, G. Li, and Z. Bie, "A new model for resilient distribution systems by microgrids formation," *IEEE Trans. Power Syst.*, vol. 32, no. 5, pp. 4145–4147, Sep. 2017.
[32] A. Papavasiliou, "Analysis of distribution locational marginal prices," *IEEE Trans. Smart Grid*, vol. 9, no. 5, pp. 4872–4882, Sep. 2018.
[33] M. Lubin and I. Dunning, "Computing in operations research using Julia," *INFORMS J. Comput.*, vol. 27, no. 2, pp. 238–248, 2015.
[34] J. Kim and Y. Dvorkin. (2018). *Code Supplement for Enhancing Distribution System Resilience With Mobile Energy Storage and Microgrids*. [Online]. Available: https://github.com/jipkim/MES_resilience
[35] K. P. Schneider *et al.*, "Analytic considerations and design basis for the IEEE distribution test feeders," *IEEE Trans. Power Syst.*, vol. 33, no. 3, pp. 3181–3188, May 2018.

Jip Kim received the B.S. degree in electrical and electronic engineering from Yonsei University, Seoul, South Korea, in 2012 and the M.S. degree in electrical and computer engineering from Seoul National University, Seoul, South Korea, in 2014. He is currently pursuing the Ph.D. degree with the Smart Energy Research Group, New York University, NY, USA, where he is an Ernst Weber Fellow with the Department of Electrical and Computer Engineering. His research focuses on developing mathematical models and optimization algorithms to solve power system engineering problems.

Yury Dvorkin received the Ph.D. degree from the University of Washington, Seattle, WA, USA, in 2016. He is currently an Assistant Professor with the Department of Electrical and Computer Engineering, New York University, NY, USA. His research interests include short- and long-term planning in power systems with renewable generation and power system economics. He was a recipient of the 2016 Scientific Achievement Award by Clean Energy Institute (University of Washington) for his Doctoral dissertation "Operations and Planning in Sustainable Power Systems."